ARTICLE

Supercapacitive Properties of PEDOT and Carbon Colloidal Microspheres

Timothy L. Kelly,[†] Kazuhisa Yano,[‡] and Michael O. Wolf*[,†]

Department of Chemistry, University of British Columbia, Vancouver, British Columbia V6T 1Z1, Canada, and Toyota Central R&D Laboratories, Inc., Nagakute, Aichi 480-1192, Japan

ABSTRACT The synthesis and characterization of a new PEDOT−carbon composite prepared using a microporous carbon template are described. The electrochemical behavior of this composite, as well as that of three other colloidal materials—PEDOT−silica, PEDOT, and microporous carbon particles—is investigated with respect to their suitability as electrode materials in supercapacitors. This was accomplished by a combination of cyclic voltammetry and galvanostatic charge/discharge cycles. It was found that the PEDOT−silica composite had the lowest specific capacitance of the four materials (ca. 60 F g^{-1}) and also the worst retention of the capacitance at high scan rates. In the case of pure PEDOT, microporous carbon, or PEDOT−carbon microspheres, the specific capacitances of the materials were dramatically higher (C_M = 115, 109, and 106 F g^{-1}, respectively). These values are higher than those of either unstructured electropolymerized PEDOT or commercially available high-surface-area carbon. The pure PEDOT materials retained this high capacitive behavior even at faster scan rates, although the capacitance of the carbon and PEDOT−carbon microspheres dropped substantially. These results are interpreted in the context of the local microstructure of the individual colloidal particles, as well as the overall film morphology. The morphologies of both the individual particles and the electrode films were investigated by field-emission scanning electron microscopy. Due to the monodisperse nature of the microspheres, films composed of these materials necessarily possess an interconnected network of interstitial pores that allow for facile ionic diffusion. This allows for more penetration of the conjugated polymer by the ionic electrolyte and therefore higher capacitances relative to the bulk materials. These results demonstrate the feasibility of utilizing monodisperse colloidal microparticles containing conjugated polymers as electrode materials for high-energy and high-power-density supercapacitors.

KEYWORDS: carbon • conjugated polymers • PEDOT • supercapacitors • colloids

INTRODUCTION

Conjugated polymers have shown substantial promise for application in the next generation of organic electronic devices. The electronic and electrochemical behavior of these materials is now relatively well understood, and the next frontier is to develop the ability to control their morphology and microstructure. These properties can affect the efficiency, longevity, and response time of devices such as photovoltaic cells (1), organic light-emitting diodes (2), electrochemical transistors (3) and electrochromic displays (4).

One of the emerging applications of such conjugated polymer nanostructures is as electrode materials for supercapacitors. Supercapacitors are becoming an important class of energy storage devices because of their high power density (5). As such, they have found use in situations where large energy demands are made in a short period of time, such as in electric vehicles and portable electronic devices. Materials such as porous carbon (6, 7), transition-metal oxides (8), and conjugated polymers (9−12) are all commonly employed in the fabrication of supercapacitors. Of these, conjugated polymers have the advantage of being able to store charge not just in the electrical double layer but also throughout the body of the polymer by rapid faradaic charge transfer (pseudocapacitance). While this is also true of transition-metal oxides, these materials typically suffer from poor electrical conductivity. In contrast, conjugated polymers typically have good conductivity in their doped state; they also display fast, reversible, and stable electrochemical behavior. Among conjugated polymers, poly(3,4-ethylenedioxythiophene) (PEDOT) has been extensively exploited as a charge-storage material (12−14). While the mass-specific capacitance (C_M) of PEDOT is typically lower than those of other conjugated polymers (e.g., polyaniline and polypyrrole), its high stability with respect to repeated cycling makes it very suitable as a potential supercapacitor material.

Recent research has focused on improving both the energy and power density of PEDOT-based supercapacitors. Since the charging and discharging of PEDOT involves the mass transport of counterions into and out of the polymer film (Scheme 1), the rate of ion diffusion is often one of the limiting factors in the efficiency of PEDOT-based supercapacitors. Thus, improvements in both the energy and power density have been achieved by preparing nanostructured, high-surface-area electrodes and limiting the distance over which ion diffusion must occur.

A wide variety of approaches have been adopted in the preparation of conjugated polymer micro- and nanostructures. These include the use of templates such as surfactant micelles (15, 16), zeolites (17, 18), mesoporous silicas

* E-mail: mwolf@chem.ubc.ca.
Received for review August 26, 2009 and accepted October 14, 2009
[†] University of British Columbia.
[‡] Toyota Central R&D Laboratories, Inc.
DOI: 10.1021/am900575v

Published on Web 11/04/2009

Scheme 1. Charging (Oxidation) and Discharging (Reduction) of PEDOT[a]

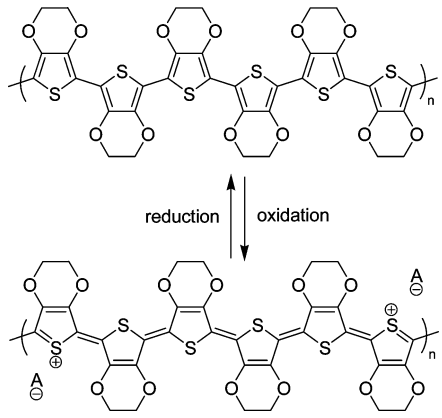

[a] Counterions (anions) are denoted as A^-.

(19, 20), porous alumina (21, 22) and polymer latexes (23–25). The use of such structure-directing templates enables access to a variety of morphologies, including nanoparticles (26, 27), microspheres (23–25), nanowires (28, 29) and mesocellular foams (15).

A number of groups have prepared PEDOT electrodes in this manner. Li et al. examined the effects of ultrasonication on the chemical synthesis of PEDOT and found a moderate increase in the specific capacitance of the polymer due to an increase in the porosity (30). PEDOT–carbon nanotube composites have also been shown to possess good mass-specific capacitance because of the interconnected high-surface-area network of carbon nanotubes (31). Jang et al. have prepared mesocellular foams based on PEDOT (15). In a similar fashion, the high interfacial surface area leads to rapid ion diffusion and a high value for the specific capacitance. Lee and co-workers have extensively developed hollow PEDOT nanotubes (32–34); because of the extremely thin nature of the polymer tube (on the order of nanometers), ions diffuse into and out of the polymer extremely rapidly. This leads to very high energy and power densities.

Previous work in our laboratory has focused on preparing highly monodisperse PEDOT–silica and PEDOT microspheres (35). This morphology offers a potentially interesting platform for the study of supercapacitive behavior, in that densely packed arrays of such microspheres have a network of continuous interstitial voids that should allow for the rapid diffusion of ions. Additionally, Yano and co-workers have reported the synthesis of monodisperse, microporous, carbon microspheres (36). The hierarchical combination of macro- (the interstitial voids) and microporosity (within individual microspheres) may allow for extremely fast ion transport within the electrode film. In this report, we describe the synthesis and characterization of a new PEDOT–carbon composite. We have also evaluated the electrochemical behavior of each of these materials—PEDOT–silica, PEDOT, microporous carbon, and PEDOT–carbon microspheres—for their potential utility in supercapacitors. Films composed of the PEDOT microspheres yielded both the highest energy and power densities of the four samples and were found to have a mass-specific capacitance superior to that of ordinary PEDOT films. It was also found that the microporous carbon spheres possess a high specific capacitance relative to common, commercially available carbon preparations. This indicates that the high level of control over the local microstructure has a pronounced influence on the overall efficiency and usability of the materials.

EXPERIMENTAL SECTION

Materials. 3,4-Ethylenedioxythiophene (EDOT) was donated by Bayer, vacuum-distilled, and stored at 4 °C under a nitrogen atmosphere. *N*-Methylpyrrolidinone (NMP), poly(vinylidene fluoride) (PVDF; $M_w \sim 275\,000$), and sodium persulfate (98%) were purchased from Sigma-Aldrich and used as received. Concentrated sulfuric acid was purchased from Fisher Scientific and used to prepare a 1 M aqueous solution. The PEDOT (35), PEDOT–silica (35), and microporous carbon spheres (36) were prepared according to literature procedures.

General Characterization. Pore volumes were measured on a Quantachrome Autosorb-1 analyzer at 77 K using nitrogen gas. Field-emission scanning electron microscopy (FE-SEM) images were taken on a Hitachi S-4700 microscope operating between 1.0 and 5.0 kV, and energy-dispersive X-ray analysis (EDX) was conducted on a Hitachi S-3000N microscope operating at 20.0 kV. The EDX used conventional ZAF correction factors to correct for matrix effects. Particle size distributions were determined by FE-SEM analysis with a minimum sample size of 200 particles. Thermogravimetric analysis (TGA) was carried out on a Pyris 6 system.

Electrochemical Characterization. Working electrodes were made by dispersing an accurately known amount (10–15 mg) of colloidal microspheres in a solution (1.00 mL) of poly(vinylene difluoride) in NMP (0.0112 g mL^{-1}). From this stock dispersion, a small amount (50 μL) was pipetted onto the end of a stainless steel plate (1 × 3 cm) and dried at 130 °C for 16 h. Cyclic voltammetry (CV) and galvanostatic charge/discharge experiments were carried out using a three-electrode setup, which consisted of the modified stainless steel working electrode, a platinum mesh counter electrode, and a 3 M Ag/AgCl reference electrode. A 1 M solution of sulfuric acid was used as the electrolyte. Potentials/currents were applied using an Autolab potentiostat/galvanostat.

PEDOT–Carbon Synthesis. Microporous carbon spheres (0.100 g) were placed in a Schlenk tube and dried at 120 °C under vacuum for 2 h. The atmosphere was replaced with nitrogen gas, and enough EDOT to completely fill the pore volume of the microporous carbon (105 μL) was added. The mixture was agitated with a spatula for 6 min and then annealed at 60 °C for 1 h. The black powder was then stirred in a solution of sodium persulfate (0.15 g) in water (3.00 mL) at room temperature for 16 h. The solid material was isolated by centrifugation and washed by redispersion/centrifugation cycles using water (1 × 15 mL), ethanol (2 × 15 mL), and water (1 × 15 mL). Drying at 60 °C for 5 h yielded the PEDOT–carbon composite as a black powder (0.18 g).

RESULTS AND DISCUSSION

Synthesis and Characterization. The syntheses of the PEDOT, PEDOT–silica, and microporous carbon materials were accomplished by an infiltration and in situ polymerization approach that had been previously reported (35, 36). In order to introduce PEDOT into the micropores of the carbon template, a similar approach was adopted. The carbon microspheres were first dried at 120 °C under vacuum in order to remove adsorbed water. The pores were

Scheme 2. Synthesis of the PEDOT−Carbon Composite by Infiltration of the Monomer (EDOT) and Subsequent Oxidative Polymerization

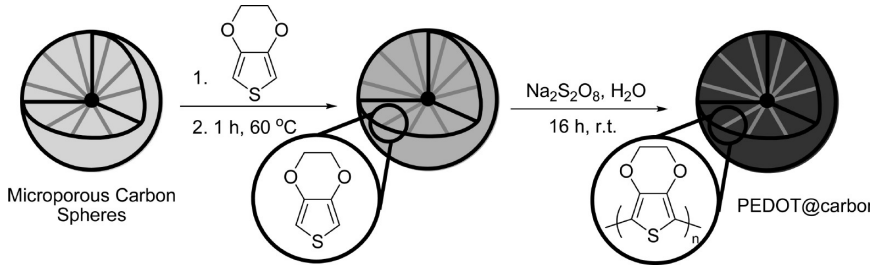

then filled with EDOT by capillary action, and EDOT was polymerized by the addition of sodium persulfate (an oxidizing agent). This process is shown in Scheme 2.

The amount of redox-active polymer present in each of the materials is the first important parameter to quantify for each of the samples. This was determined by a combination of TGA and EDX. The TGA curves of the carbon and PEDOT−carbon samples are shown in Figure 1, while the TGA curves of the PEDOT−silica and PEDOT samples were reported previously (35). From Figure 1, it can be seen that for the microporous carbon spheres the onset of decomposition occurs at ca. 500 °C and that decomposition is complete by 750 °C. After the carbon template has been filled with PEDOT, the decomposition process occurs in a series of discrete steps. The first mass loss (8%) occurs at 100 °C. This is typical of adsorbed moisture and has also been observed in the PEDOT−silica and PEDOT composites (35). A second loss of ca. 27% occurs between 200 and 450 °C with an inflection point at 350 °C. This may be due to (partial) decomposition of PEDOT; because decomposition of PEDOT should occur in the range of 300−600 °C (35), it is unlikely that all of the PEDOT has been lost by 450 °C in the PEDOT−carbon sample. The temperature range of 450−900 °C sees a continual, gradual loss of material from the PEDOT−carbon sample. Some of this mass loss is likely due to residual PEDOT decomposition, while the remainder is due to combustion of the carbon template. TGA of the PEDOT−silica and PEDOT microspheres reveals mass losses

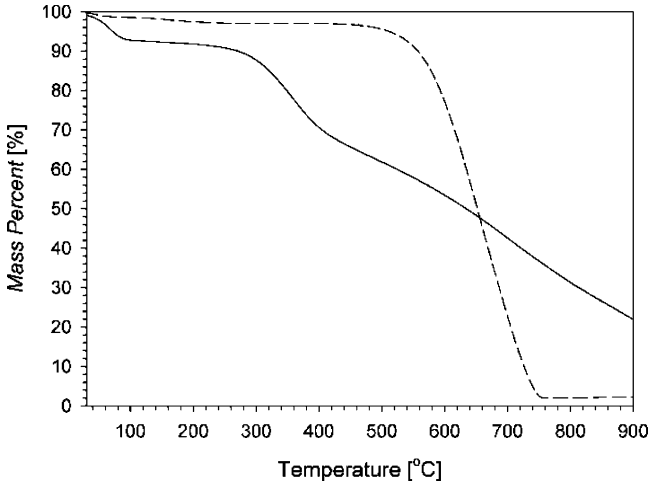

FIGURE 1. TGA of the microporous carbon spheres (dashed line) and the PEDOT−carbon composite (solid line).

(50% for PEDOT−silica and 100% for PEDOT) between 300 and 600 °C that are easily attributable to decomposition of the conjugated polymer.

While the PEDOT−silica, PEDOT, and carbon materials are straightforward to analyze by TGA, the results for the PEDOT−carbon composite are more ambiguous. EDX was carried out in order to obtain more quantitative results. The EDX data are shown in Table S1 in the Supporting Information; importantly, the analysis reveals a 12% (w/w) sulfur concentration in the sample. If it is assumed that all of the sulfur present is due to the presence of PEDOT, then this would indicate that, in addition to the 12% of sulfur content, 12% of the total mass of the sample is due to the PEDOT oxygen atoms and 27% due to the PEDOT carbon atoms. The remaining oxygen is also present in the carbon template and is likely due to the alcohol, aldehyde, or carboxylic acid functionalities. These data are consistent with the TGA results, which indicated that the composite was >27% PEDOT. From both TGA and EDX data, it can be concluded that the carbon and PEDOT microspheres are essentially pure materials, whereas the PEDOT−carbon and PEDOT−silica microspheres are both approximately 50% PEDOT by mass.

Particle Morphology. The suitability of each of these materials for supercapacitor applications will be dictated at least partly by their morphology; high-magnification FE-SEM micrographs of each of the four colloidal materials are shown in Figure 2. Previous work has shown that the PEDOT−silica composite consists of monodisperse, spherical particles with a diameter of 730 ± 35 nm. The surface texture visible in Figure 2a is due to a layer of PEDOT present on the surface of the particles. It is this surface layer that is responsible for making electrical connections between both adjacent particles and with the current collector in a working device. Figure 2b shows the micrograph of the PEDOT microspheres after removal of the silica template with hydrofluoric acid. The diameter of these particles is 670 ± 32 nm; the free volume that would have been present because of the removal of the template is lost upon etching due to collapse of the particle structure. The microporous carbon particles (Figure 2c) are also quite spherical and monodisperse in diameter ($d = 321 \pm 20$ nm). The surface texture visible on the particles is due to the presence of radially aligned micropores that extend outward from the center of each particle. The presence of this microporosity was confirmed by nitrogen adsorption measurements (Figure S1 in the

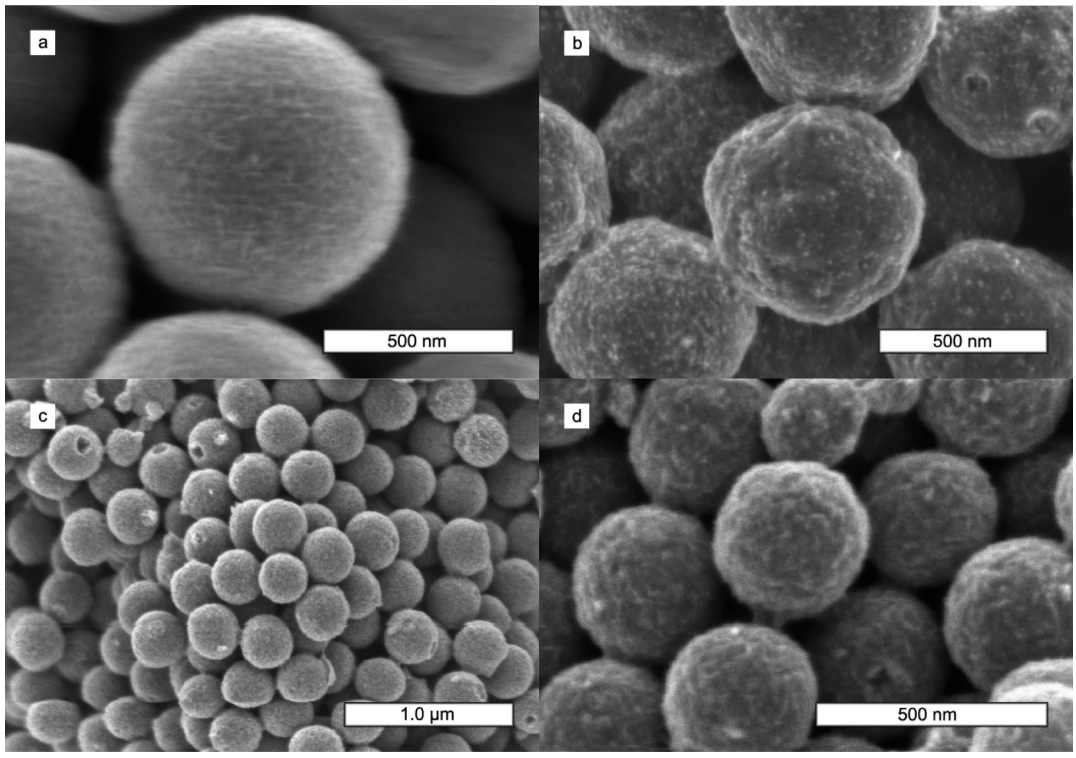

FIGURE 2. FE-SEM micrographs of the (a) PEDOT−silica, (b) PEDOT, (c) microporous carbon, and (d) PEDOT−carbon materials.

Supporting Information); the high surface area of the carbon microspheres (S_{BET} = 1600 m^2 g^{-1}) might therefore be expected to lead to a large value for the specific capacitance. In the PEDOT−carbon composite, this void space has been filled with PEDOT. The diameter of the composite (d = 326 ± 19 nm) is essentially the same as that of the carbon template.

Electrochemistry. The capacitance of each of the four materials was initially evaluated by CV. The cyclic voltammograms are shown in Figure 3. Importantly, the voltammograms display good capacitive behavior, with a sharp rise in the current at low voltages, followed by a sharp drop at the vertex potential. In the case of the PEDOT-containing materials, this is due to the generation and destruction of charge carriers on the polymer backbone and the concomitant in- and out-flow of anions (Scheme 1). For the microporous carbon spheres, the current is simply due to the charging of the electrical double layer. At fast scan rates (>25 mV s^{-1}), each of the four sets of voltammograms has a similar, distorted rectangular shape. This deviation from ideal behavior is indicative of an uncompensated resistance in the system. At higher scan rates, the currents are correspondingly higher, leading to a more pronounced iR loss. The uncompensated resistance may be due to imperfect contact between the active electrode material and the stainless steel current collector, which is a well-known issue in electrodes of this type. The effect may be more pronounced because of the lack of any carbon black to improve the conductivity of the electrode film.

When the electrochemistries of the various materials are compared, several differences are immediately apparent. First, in the case of the PEDOT−silica composite, the widths of the voltammograms (the difference between the anodic and cathodic plateau currents) are much smaller than they are in the case of the pure PEDOT analogues. The width of the voltammogram is directly related to the mass-specific capacitance of the material by eq 1.

$$C_M = \frac{i}{\left(\frac{\Delta V}{\Delta t}\right) m_e} \quad (1)$$

The currents obtained at 1 mV s^{-1} can be directly converted into capacitance values by eq 1, and the results are shown in Figure 4a. At these slow scan rates, additional detail in the voltammograms can be resolved. For the PEDOT−silica material, a faint oxidation peak can be observed at 0.6 V, and the reverse reduction wave is visible at 0.25 V. These peaks may be due to the oxidation and reduction of PEDOT; similar peaks were observed by Jang et al. in their electrochemical study of PEDOT nanoparticles (15). These peaks can still be observed but are no longer as prominent in the pure PEDOT sample, which displays a more rectangular voltammogram. The carbon and PEDOT−carbon samples display similar electrochemical behavior. Both voltammograms resemble slightly distorted rectangles, indicative of a capacitive behavior with a slight uncompensated resistance.

The specific capacitances of the four materials are plotted as a function of the scan rate in Figure 4b. It can be seen that the maximum capacitance of the PEDOT microspheres is nearly twice that of the PEDOT−silica composite (115 F g^{-1} as compared to 62 F g^{-1}). In light of the elemental analysis data presented in Figure S1 and Table S1 in the Supporting Information, these values are in reason-

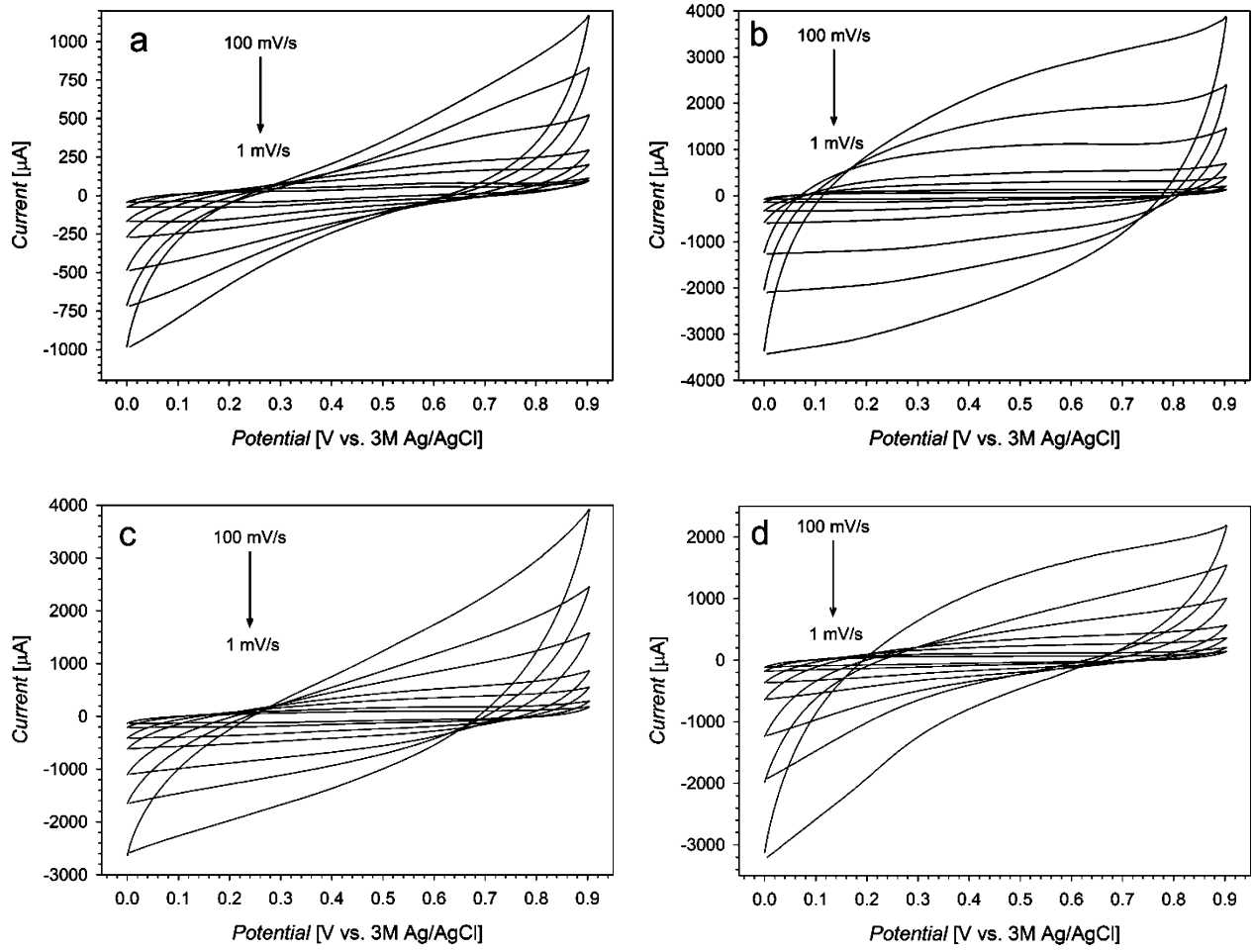

FIGURE 3. Cyclic voltammograms at scan rates of 1, 2, 5, 10, 25, 50, and 100 mV s^{-1} for the (a) PEDOT−silica, (b) PEDOT, (c) microporous carbon, and (d) PEDOT−carbon materials.

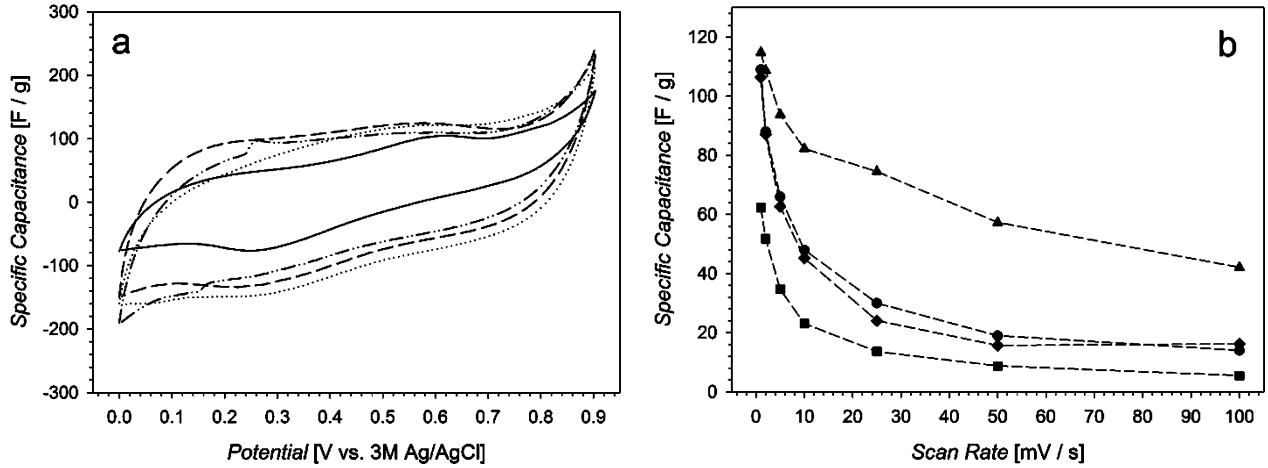

FIGURE 4. (a) Cyclic voltammograms recorded at 1 mV s^{-1} for the PEDOT−silica (solid line), PEDOT (dashed line), carbon (dotted line), and PEDOT−carbon (dash-dotted line) materials. The *y* axis has been converted to the specific capacitance. (b) Mass-specific capacitance of the PEDOT−silica (squares), PEDOT (triangles), carbon (circles), and PEDOT−carbon (diamonds) composites as a function of the scan rate. The dashed connecting lines are meant to guide the eye.

able agreement; the PEDOT−silica composite contains approximately 50% (w/w) of an electrochemically inactive material (silica), and therefore on a mass basis the specific capacitance is expected to be roughly half that of the pure PEDOT analogue. Importantly, however, the presence of the silica template has a dramatic effect on the overall usability of the material. As the scan rate is increased, the specific capacitance of the PEDOT−silica material drops dramatically; in contrast, the capacitance of the PEDOT microparticles shows a much more gradual decline. As the scan rate approaches 50 mV s^{-1}, the PEDOT microparticles retain approximately 50% of their maximum total capacitance, whereas the PEDOT−silica microparticles have lost almost all of their capacitive ability.

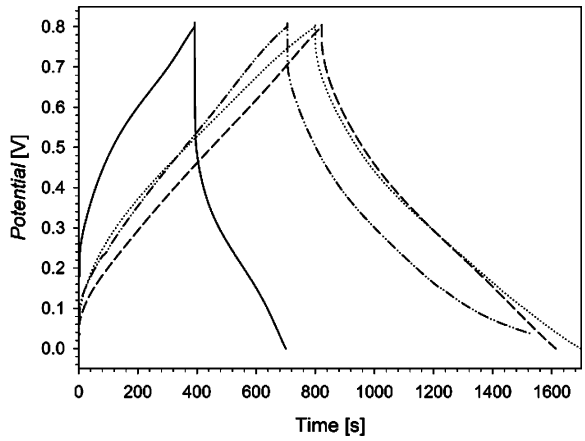

FIGURE 5. Normalized galvanostatic charge/discharge cycles recorded at 0.1 mA for the PEDOT−silica (solid line), PEDOT (dashed line), microporous carbon (dotted line), and PEDOT−carbon (dash-dotted line) microspheres.

This behavior is also reflected in the data for the carbon and PEDOT−carbon samples. The microporous carbon spheres have a maximum specific capacitance of 109 F g^{-1}, which is larger than that of commercially available high-surface-area carbon (37, 38) and competitive with many recent state-of-the-art examples. For example, carbon-inverted opal structures have been shown to have specific capacitances in the range of 64−127 F g^{-1} (7), while Largeot et al. reported capacitances of 100−160 F g^{-1} in an optimization study of microporous carbon in an ionic liquid electrolyte (6). The incorporation of PEDOT into the carbon template does not dramatically influence the capacitance of the material, and the specific capacitance (C_M = 106 F g^{-1}) is very similar to that of the pure carbon microspheres. This suggests that the additional charge-storage capacity provided by the addition of the redox-active polymer is offset by the elimination of microporosity in the composite (Figure S1 in the Supporting Information). In both the carbon and PEDOT−carbon materials, the specific capacitance of the sample decreases sharply with an increase in the scan rate. This is especially evident when compared to the PEDOT microspheres, which have a much more constant specific capacitance.

In order to further probe the capacitive behavior of these materials, the electrode films were subjected to galvanostatic charge/discharge experiments. The data recorded at 0.1 mA are shown in Figure 5. As expected from the CV results, the PEDOT−silica material performed relatively poorly. The charging and discharging cycle deviated markedly from the ideal triangular shape of a capacitor, and the discharge time was short, indicating a low specific capacitance. The other three materials displayed more promising behavior. Aside from a small *iR* drop, the PEDOT microspheres exhibited a very triangular charge/discharge cycle and a lengthy discharge time. The data for the microporous carbon closely mirror those for the PEDOT spheres, and while the data for the PEDOT−carbon composite are slightly less than ideal, the total discharge time is long. The specific capacitances obtained from these data are tabulated in Table 1, along with the values obtained by CV.

Table 1. Mass-Specific Capacitances C_M (F g^{-1}) Obtained from CV and Galvanostatic Experiments

	PEDOT−silica	PEDOT	carbon	PEDOT−carbon
galvanostatic	39	99	112	102
CV	62	115	109	106

The specific capacitances of the PEDOT−silica and PEDOT microspheres determined by the galvanostatic experiments are similar to, but slightly lower than, those measured by CV. This observation can be explained by the fact that the value of C_M measured by CV is reported at one particular potential, while that obtained by galvanostatic cycling is an average capacitance for the potential range of 0−0.8 V. From Figure 4a, it can be seen that the overall width of the voltammogram is wider in the lower half of the voltage range studied and narrower at the upper limit. Thus, averaging the capacitances over the entire voltage range leads to the observed decrease. The specific capacitances of the carbon and PEDOT−carbon microspheres, as determined galvanostatically, are the same as those determined by CV (within experimental error). This finding is in agreement with the more rectangular voltammograms observed for these materials (Figure 4a).

Film Morphology. In order to explain the differences in the electrochemical behavior between the four samples, the electrode films were subjected to analysis by FE-SEM. Parts a and b of Figure 6 show the film morphologies of the PEDOT−silica and PEDOT-based electrodes, respectively. In Figure 6a, there are areas of low film coverage where the steel substrate can be seen (light gray), although most of the field of view is thickly covered by the PEDOT−silica microspheres (dark gray). The PEDOT−silica film appears to have semiregular pores (black areas) penetrating into the film. These are due to the disordered nature of the film; a close-packed array of colloidal microspheres would be expected to possess no such porosity. The film morphology of the PEDOT microspheres is similar, with a high degree of porosity (black areas) interspersed in a PEDOT matrix (gray areas). In both cases, the pore diameters are roughly 1−2 μm in size (approximately 1−3 particle diameters). Despite the similarities of the film morphology, however, the PEDOT−silica materials exhibited a much sharper decrease in capacitance with an increase in the scan rate. This is likely due to restrictions on ion diffusion within the individual microparticles. The silica template provides an impermeable barrier to ions, forcing them to follow very narrow, defined pathways through the particle; once an ion has entered the body of a pore, it can diffuse only in the radial direction. In contrast, in the case of the PEDOT microspheres, the ions are free to migrate throughout the bulk of the particles. This is schematically illustrated in Figure 7.

Parts c and d of Figure 6 show the film morphologies of the microporous carbon and PEDOT−carbon electrodes. The morphologies are markedly different from those of the PEDOT−silica and PEDOT electrodes. Rather than a smooth, macroporous film, the individual particles form large aggregates that are between 10 and 50 μm in size. This aggregation is less pronounced for the PEDOT−carbon

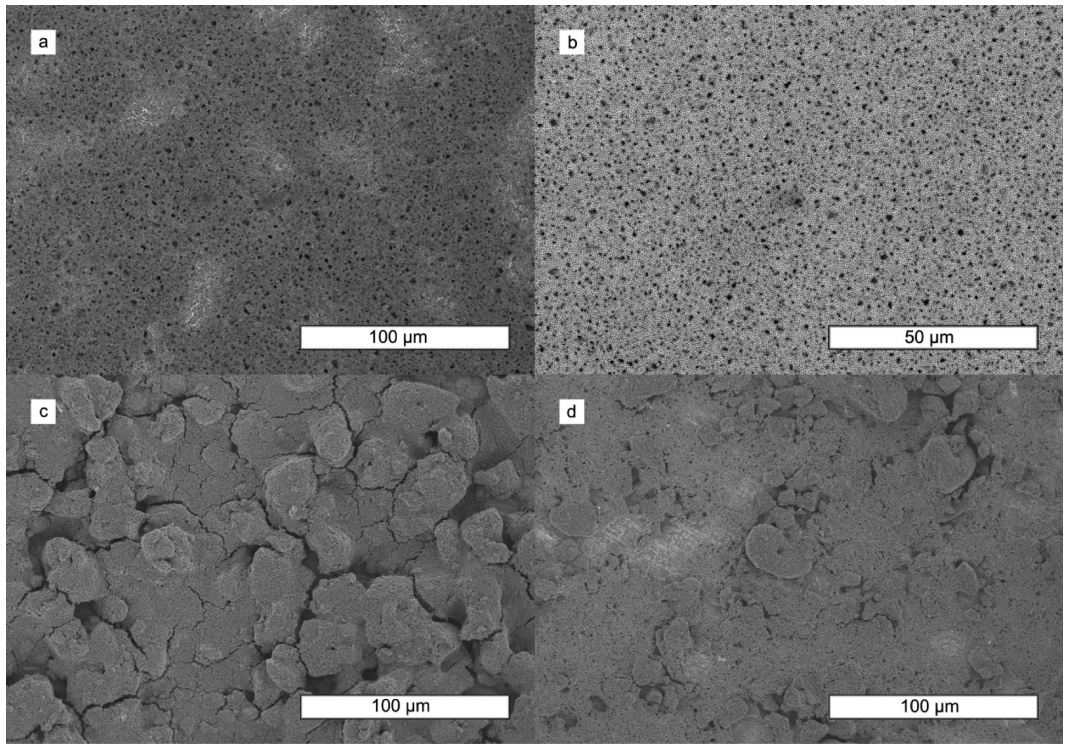

FIGURE 6. FE-SEM micrographs of the electrodes made of (a) PEDOT−silica/PVDF, (b) PEDOT/PVDF, (c) carbon/PVDF, and (d) PEDOT−carbon/PVDF.

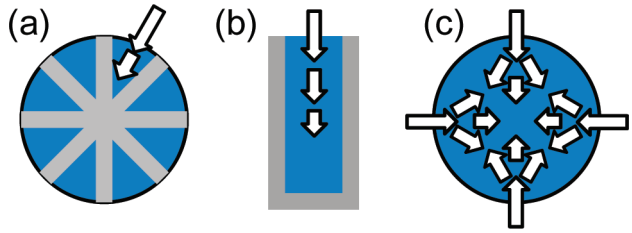

FIGURE 7. Schematic illustration of ion diffusion within (a) an individual PEDOT−silica particle, (b) a single mesopore of the particle shown in part a, and (c) an individual PEDOT microsphere. Possible routes for ion diffusion are indicated by white arrows. Silica is shown in gray and PEDOT in blue.

sample but is, nonetheless, still present. In contrast to films composed of the PEDOT microspheres, the clustering of the particles and the lack of semiregular porosity in the film may limit the rate of ion diffusion. In turn, this may lead to the observed drop-off in the specific capacitance of the electrode at higher scan rates. Alternatively, it may be the ion diffusion within an individual particle that is the limiting factor in maintaining high capacitance at faster scan rates.

CONCLUSIONS

In summary, we have reported the synthesis of a PEDOT−carbon composite material and investigated the suitability of a series of colloidal microspheres for use as supercapacitor electrode materials. Of the four materials under study, the PEDOT and microporous carbon materials exhibited the highest specific capacitances, and it was demonstrated that the PEDOT microparticles retained much of their capacitive properties at higher scan rates. FE-SEM investigations suggested that this may be due to the semiregular, macroporous nature of the electrode film, which would allow for facile ion diffusion throughout the material. This report demonstrates the feasibility of using submicrometer colloidal microspheres to introduce porosity into an electrode film through an interconnected sequence of interstitial voids and micrometer-sized macropores. It also demonstrates the subsequent effect on the specific capacitances of the materials under study, namely, an increase in capacitance relative to the bulk materials. An in-depth study of ion diffusion within the carbon and PEDOT microspheres is ongoing and will be reported at a later date.

Acknowledgment. The financial support of Toyota Central R&D Laboratories, Inc., is gratefully acknowledged. T.L.K. thanks the Natural Sciences and Engineering Research Council of Canada (NSERC) for a scholarship.

Supporting Information Available: Nitrogen adsorption isotherms of the microporous carbon spheres and the PEDOT−carbon composites and EDX analyses of the microporous carbon and PEDOT−carbon microspheres. This material is available free of charge via the Internet at http://pubs.acs.org.

REFERENCES AND NOTES

(1) Thompson, B. C.; Frechet, J. M. J. *Angew. Chem., Int. Ed.* **2008**, *47*, 58–77.
(2) Jenekhe, S. A.; Zhang, X.; Chen, X. L.; Choong, V.-E.; Gao, Y.; Hsieh, B. R. *Chem. Mater.* **1997**, *9*, 409–412.
(3) Bernards, D. A.; Malliaras, G. G. *Adv. Funct. Mater.* **2007**, *17*, 3538–3544.
(4) Cho, S. I.; Kwon, W. J.; Choi, S.-J.; Kim, P.; Park, S.-A.; Kim, J.; Son, S. J.; Xiao, R.; Kim, S.-H.; Lee, S. B. *Adv. Mater.* **2005**, *17*, 171–175.
(5) Winter, M.; Brodd, R. J. *Chem. Rev.* **2004**, *104*, 4245–4269.
(6) Largeot, C.; Portet, C.; Chmiola, J.; Taberna, P.-L.; Gogotsi, Y.; Simon, P. *J. Am. Chem. Soc.* **2008**, *130*, 2730–2731.

(7) Moriguchi, I.; Nakahara, F.; Furukawa, H.; Yamada, H.; Kudo, T. *Electrochem. Solid-State Lett.* **2004**, *7*, A221–A223.
(8) Ghodbane, O.; Pascal, J.-L.; Favier, F. *ACS Appl. Mater. Interfaces* **2009**, *1*, 1130–1139.
(9) Fan, L.-Z.; Hu, Y.-S.; Maier, J.; Adelhelm, P.; Smarsly, B.; Antonietti, M. *Adv. Funct. Mater.* **2007**, *17*, 3083–3087.
(10) Li, H.; Wang, J.; Chu, Q.; Wang, Z.; Zhang, F.; Wang, S. *J. Power Sources* **2009**, *190*, 578–586.
(11) Muthulakshmi, B.; Kalpana, D.; Pitchumani, S.; Renganathan, N. G. *J. Power Sources* **2006**, *158*, 1533–1537.
(12) Snook, G. A.; Peng, C.; Fray, D. J.; Chen, G. Z. *Electrochem. Commun.* **2006**, *9*, 83–88.
(13) Carlberg, J. C.; Inganäs, O. *J. Electrochem. Soc.* **1997**, *144*, L61–L64.
(14) Patra, S.; Munichandraiah, N. *J. Appl. Polym. Sci.* **2007**, *106*, 1160–1171.
(15) Jang, J.; Bae, J.; Park, E. *Adv. Mater.* **2006**, *18*, 354–358.
(16) Landfester, K.; Montenegro, R.; Scherf, U.; Guntner, R.; Asawapirom, U.; Patil, S.; Neher, D.; Kietzke, T. *Adv. Mater.* **2002**, *14*, 651–655.
(17) Bein, T.; Enzel, P. *Angew. Chem., Int. Ed. Engl.* **1989**, *28*, 1692–1694.
(18) Enzel, P.; Bein, T. *J. Phys. Chem.* **1989**, *93*, 6270–6272.
(19) Cheng, Q.; Pavlinek, V.; Lengalova, A.; Li, C.; Belza, T.; Saha, P. *Microporous Mesoporous Mater.* **2006**, *94*, 193–199.
(20) Nguyen, T.-Q.; Wu, J.; Doan, V.; Schwartz, B. J.; Tolbert, S. H. *Science* **2000**, *288*, 652–656.
(21) Han, M. G.; Foulger, S. H. *Chem. Commun.* **2005**, 3092–3094.
(22) Xiao, R.; Cho, S. I.; Liu, R.; Lee, S. B. *J. Am. Chem. Soc.* **2007**, *129*, 4483–4489.
(23) Han, M. G.; Foulger, S. H. *Adv. Mater.* **2004**, *16*, 231–234.
(24) Han, M. G.; Foulger, S. H. *Chem. Commun.* **2004**, 2154–2155.
(25) Khan, M. A.; Armes, S. P. *Langmuir* **1999**, *15*, 3469–3475.
(26) Jang, J.; Oh, J. H.; Stucky, G. D. *Angew. Chem., Int. Ed.* **2002**, *41*, 4016–4019.
(27) Müller, K.; Klapper, M.; Müllen, K. *Macromol. Rapid Commun.* **2006**, *27*, 586–593.
(28) Abidian, M. R.; Kim, D.-H.; Martin, D. C. *Adv. Mater.* **2006**, *18*, 405–409.
(29) Zhang, L.; Peng, H.; Kilmartin, P. A.; Soeller, C.; Travas-Sejdic, J. *Macromolecules* **2008**, *41*, 7671–7678.
(30) Li, W.; Chen, J.; Zhao, J.; Zhang, J.; Zhu, J. *Mater. Lett.* **2005**, *59*, 800–803.
(31) Frackowiak, E.; Khomenko, V.; Jurewicz, K.; Lota, K.; Beguin, F. *J. Power Sources* **2006**, *153*, 413–418.
(32) Cho, S. I.; Lee, S. B. *Acc. Chem. Res.* **2008**, *41*, 699–707.
(33) Liu, R.; Cho, S. I.; Lee, S. B. *Nanotechnology* **2008**, *19*, 215710/1–215710/8.
(34) Liu, R.; Lee Sang, B. *J. Am. Chem. Soc.* **2008**, *130*, 2942–2943.
(35) Kelly, T. L.; Yamada, Y.; Che, S. P. Y.; Yano, K.; Wolf, M. O. *Adv. Mater.* **2008**, *20*, 2616–2621.
(36) Nakamura, T.; Yamada, Y.; Yano, K. *Microporous Mesoporous Mater.* **2009**, *117*, 478–485.
(37) Barbieri, O.; Hahn, M.; Herzog, A.; Koetz, R. *Carbon* **2005**, *43*, 1303–1310.
(38) Zhou, H.; Zhu, S.; Hibino, M.; Honma, I. *J. Power Sources* **2003**, *122*, 219–223.

AM900575V